# Enzyme Electrokinetics: Energetics of Succinate Oxidation by Fumarate Reductase and Succinate Dehydrogenase†

Christophe Léger,‡ Kerensa Heffron,‡ Harsh R. Pershad,§ Elena Maklashina,|| César Luna-Chavez,||,⊥ Gary Cecchini,|| Brian A. C. Ackrell,|| and Fraser A. Armstrong*,‡

*Inorganic Chemistry Laboratory, Oxford OX1 3QR, U.K., Department of Chemistry, University of California at Berkeley, Berkeley, California 94720, Molecular Biology Division, VA Medical Center and Department of Biochemistry and Biophysics, University of California, San Francisco, California 94121*

*Received May 1, 2001; Revised Manuscript Received July 6, 2001*

ABSTRACT: Protein film voltammetry is used to probe the energetics of electron transfer and substrate binding at the active site of a respiratory flavoenzyme—the membrane-extrinsic catalytic domain of *Escherichia coli* fumarate reductase (FrdAB). The activity as a function of the electrochemical driving force is revealed in catalytic voltammograms, the shapes of which are interpreted using a Michaelis−Menten model that incorporates the potential dimension. Voltammetric experiments carried out at room temperature under turnover conditions reveal the reduction potentials of the FAD, the stability of the semiquinone, relevant protonation states, and pH-dependent succinate−enzyme binding constants for all three redox states of the FAD. Fast-scan experiments in the presence of substrate confirm the value of the two-electron reduction potential of the FAD and show that product release is not rate limiting. The sequence of binding and protonation events over the whole catalytic cycle is deduced. Importantly, comparisons are made with the electrocatalytic properties of SDH, the membrane-extrinsic catalytic domain of mitochondrial complex II.

Fumarate reductase (FrdAB)[1] and succinate dehydrogenase (SDH) are the closely related water-soluble cytoplasm/matrix-facing domains of menaquinol:fumarate reductase (QFR) and succinate:ubiquinone oxidoreductase (SQR, or complex II), respectively (*1*−*5*), that catalyze redox interconversion between the dicarboxylates fumarate and succinate ($E^{0'}_{F/S} = 0-30$ mV at pH 7).

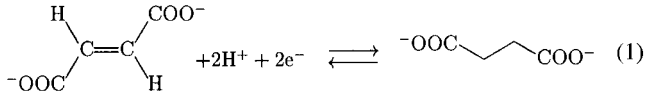


(1)

In bacteria, QFR catalyses the final step in anaerobic respiration on fumarate, coupling its reduction to succinate to the oxidation of menaquinol to menaquinone ($E^{0'}_{MQ/MQH_2} = -74$ mV). In mitochondria and other systems, SQR links the citric acid cycle to the aerobic electron-transport respiratory chain by passing the electrons from succinate to the quinone pool (ubiquinone/ubiquinol, $E^{0'}_{UQ/UQH_2} = 70-110$ mV). In vitro, both enzymes oxidize succinate or reduce fumarate using artificial electron partners. In vivo, they can replace one another functionally, following genetic manipulation of the organism (*6*, *7*).

The matrix/cytoplasm-facing peripheral domain comprises two tightly associated subunits, one containing three iron−sulfur clusters, and the other containing a 8α-($N^3$-histidyl) covalently bound flavin adenine dinucleotide (FAD) and the site for dicarboxylate binding. Whereas the crystal structure of SQR has not yet been determined, those of two QFRs [from *Escherichia coli* (*8*, *9*) and *Wolinella succinogenes* (*10*−*12*)] and of four soluble fumarate reductases (*13*−*16*) have been solved recently. In all these enzymes, dicarboxy-

† This work was supported by funds from the U.K. EPSRC and BBSRC (Grant number 43/B10492), the Department of Veterans Affairs, the National Science Foundation (MCB 9728778) and the NIH (HL-16251), and by a Fulbright-AstraZeneca award to H.R.P.

* To whom correspondence should be addressed. Phone 44-1865-272647. Fax 44-1865-272690. E-mail: fraser.armstrong@icl.ox.ac.uk.

‡ Inorganic Chemistry Laboratory.

§ Department of Chemistry.

|| Molecular Biology Division.

⊥ Current address: Center for Biophysics and Computational Biology, University of Illinois, Urbana, Illinois 61801.

[1] Abbreviations: *A*, electrode area; CHES, 2-[*N*-cyclohexylamino]-ethenesulfonic acid; DTT, threo-1,4-dimercapto-2,3-butandiol dithiothreitol; *E*, electrode potential; EGTA, ethylene glycol-bis(β-aminoethyl ether)-*N*′,*N*′,*N*′,*N*′-tetraacetic acid; $E_{O/H}$, $E_{H/R}$, One-electron reduction potentials for the two redox transitions of the flavin, see caption of Scheme 1; ET, electron transfer; [F], fumarate bulk concentrations; $\mathcal{F}$, Faraday constant; FAD, flavin adenine dinucleotide; FrdAB, fumarate reductase; Γ, electroactive coverage; HEPES, *N*-(2-hydroxyethyl)-piperazine-*N*′-[2-ethanesulfonic acid]; *i*, current; $i_{lim}$, limiting current (at high or low potential); *K*, Dissociation constant from FAD; the superscript stands for the species which binds/dissociates (e.g., "OAA", "succ", or "fum"). The subscript tells the redox state of the FAD [*O*, *H*, or *R*, for oxidized (quinone), half-reduced (semiquinone), and reduced (hydroquinone)]; $K_a$, acidity constant for the semiquinone form of the FAD; $K_m^{succ}$, $K_m^{fum}$, Michaelis constants for succinate oxidation of fumarate reduction; $k_2^{succ}$, $k_2^{fum}$, first-order potential-independent rate constants for chemical transformations in the enzyme-substrate complex (succinate oxidation by oxidized FAD or fumarate reduction depending on the superscript); κ, disproportionation constant, $\kappa = \exp(^{2\mathcal{F}}/_{RT}(E_{O/H} - E_{O/R}))$; the maximal fraction of FAD in the semiquinone form, occurring at $E = E_{O/R}$, is $\sqrt{\kappa}/(2+\sqrt{\kappa})$; M−M, Michaelis−Menten; ν, scan rate; OAA, oxaloacetate; ω, electrode rotation rate in units rpm (revolution per minute); PFV, protein film voltammetry; QFR, menaquinol:fumarate reductase; *R*, gas constants; [S], succinate bulk concentration; SDH, succinate dehydrogenase; SQR, succinate:ubiquinone oxidoreductase (complex II); *T*, temperature; TAPS, N-tris-[hydroxymethyl]methyl-3-aminopropanesulfonic acid.

10.1021/bi010889b CCC: $20.00 
Published on Web 08/23/2001

late binding utilizes hydrogen bonds from highly conserved residues, and the hydrogenation reaction is thought to involve hydride transfer between N5 of the FAD isoalloxazine ring and the substrate, followed by proton transfer (*10*). Protonation may occur via a hydrogen-bonded water molecule found in the *Wolinella* enzyme (*11*), although the *Shewanella putrefaciens* (*13*) and *Shewanella frigidimarina* (*14*, *15*) structures, along with site-directed mutagenesis (*12*, *17*−*19*), suggest that the proton donor is a conserved arginine.

The one- and two-electron reduction potentials of the active-site FAD and the resulting thermodynamic and kinetic characteristics of catalytic activity are modulated by covalent bonds with histidine (*20*, *21*) and interactions with nearby residues. Of interest here is the intrinsic bias of the enzyme toward reduction of fumarate or oxidation of succinate, an important factor being the difference between the $E^{0'}$s for FAD and fumarate: for example, in soluble fumarate reductases, the lower $E^{0'}$ of the noncovalently bound FAD contributes to make these enzymes poor catalysts of succinate oxidation. A more detailed description of the reaction requires knowing how the FAD one- and two-electron potentials depend on substrate binding (*22*−*27*). These values have been measured in equilibrium titrations but not, so far, under turnover conditions.

Protein film voltammetry (PFV) is emerging as a powerful tool to investigate redox enzymes (*28*, *29*). In this technique, the protein is adsorbed up to monolayer coverage at an electrode which effectively substitutes for the redox partner and is able to rapidly donate or abstract electrons from the enzyme depending on the electrode potential. Without substrate in solution, at slow scan rates, PFV yields equilibrium reduction potentials directly, while kinetic information can be obtained by using fast modulations of the potential (*30*). With substrate in solution, catalytic turnover produces an amplified response, the shape of which reveals details of the active-site redox transformations and the role of the driving force in controlling activity.

PFV studies of *E. coli* FrdAB (*31*, *32*) and bovine mitochondrial (*33*−*35*) and *E. coli* (*36*) SDH, as well as studies of the soluble fumarate reductases from *S. frigidimarina* (*37*−*40*) have revealed substantial differences between succinate dehydrogenases and fumarate reductases. These succinate dehydrogenases efficiently catalyze fumarate reduction, but only over a narrow potential range because activity decreases abruptly once a critical driving force is reached, i.e., at sufficiently low potential (*33*−*36*, *41*). This reversible "switch" (of possible physiological relevance) may arise from a conformational change linked to the oxidation state of FAD. By contrast, the fumarate reduction activities of *E. coli* FrdAB (at high pH) (*31*, *32*) and soluble fumarate reductases (*40*, *42*) are marked by complex sigmoidal increases upon successive reductions of the prosthetic groups.

In this paper, we describe experiments that probe and compare the catalytic energetics of FrdAB and SDH during turnover. In particular the studies reveal effects of substrate binding and roles of the different FAD redox states in catalysis.

## EXPERIMENTAL METHODS

*Purification of FrdAB and SDH. E. coli* strain DW35 [43] was transformed with plasmid pFAB-HT ($frdA^+B^+$) derived from plasmid pH3 ($frdA^+B^+C^+D^+$) (*44*). Plasmid pFAB-HT was constructed using pH3 as a template and utilizing ExSite PCR based mutagenesis (Stratagene, La Jolla, CA) to add an 8-amino acid extension (Leu-Glu-6His) to the C-terminus of the iron−sulfur protein subunit (FrdB) of fumarate reductase. The plasmid construct also resulted in deletion of the *frd*CD genes from plasmid pFAB-HT. Thus, pFAB-HT encodes soluble *E. coli* fumarate reductase with a 6His-Tag on the iron−sulfur protein subunit. To express the soluble FrdAB enzyme, *E. coli* DW35 transformed with pFAB-HT was used to inoculate 150 mL of Terrific broth (*45*) containing 150 $\mu$g/mL ampicillin in a 1-L flask and grown with vigorous aeration for 6 h. The culture was then used to inoculate 1.2 L of Terrific broth plus antibiotic in 2-L flasks and the cultures were grown with moderate aeration (200 rpm in a New Brunswick G25 rotary shaker) for 18 h at 37 °C before harvesting by centrifugation (15 min at 6000 × g). The cells were resuspended in buffer A [50 mM potassium phosphate pH 7.0, 500 mM NaCl, 1% glycerol (w/v)] and one "Complete Protease Inhibitor" tablet without EDTA (Roche, Indianapolis, IN) was added per 50 mL of suspended cells. The cells were disrupted by one passage through an Avestin homogenizer (Ottawa, Canada) at 15 000 PSI at 4 °C.

Cells and membrane fractions were removed by centrifugation at 120000×g in a Beckman Ti60 rotor for 35 min, and the supernatant was applied to nickel affinity resin (Qiagen, Chatsworth, CA) (2 × 11 cm) equilibrated with buffer A. The column was washed with 3−5 bed vol of buffer A and 2 bed volumes of buffer A with 80 mM imidazole, then FrdAB was eluted with 0.5 M imidazole. The dark-brown fractions containing the soluble FrdAB were concentrated to 2−4 mL (15−20 mg/mL) using an Amicon cell with a YM30 membrane under nitrogen, then diluted 8-fold with 20 mM histidine, 0.5 mM EDTA, 0.5 mM DTT, in 1% glycerol, pH 7.5. The resulting solution was applied to a Mono Q HR 10/10 column (Amersham Pharmacia) equilibrated with the same histidine buffer used to dilute the enzyme. The column was washed with 2 bed vol of 0.1 M KCl in the histidine buffer, then a gradient of KCl (0.1−1.0 M) was applied—the FrdAB fraction eluting at approximately 0.35 M KCl. The dark-brown fractions were pooled and brought to 60% saturation with ammonium sulfate, then precipitated by centrifugation at 20000 × g at 4 °C and stored at −80 °C. A last FPLC step was found to greatly enhance the signal intensity, resolution, and stability of the voltammetry. After passing through a PD10 column (Amersham Pharmacia) to remove ammonium sulfate, the samples were further purified anaerobically with a FPLC Mono Q column using a 0 to 0.5 M NaCl gradient (20 mM HEPES, 10% glycerol, 0.1 mM EGTA, 0.5 mM DTT, pH 7.4). Elution of the FrdAB, monitored using UV−Vis, occurred at approximately 0.3 M NaCl. Electrochemical experiments did not reveal any significant difference between the wild-type and His-tagged enzymes.

The methyl viologen-fumarate reductase assay of purified FrdAB was performed in a 2 mL cuvette, containing an argon-saturated solution of 10 mM fumarate, 200 $\mu$M methyl viologen, with glucose (10 mM), glucose oxidase and catalase to maintain anaerobiosis. Dithionite was added to reduce the viologen, and the reaction was initiated by addition of enzyme. The decrease in absorbance at 602 nm was

monitored and the rate of the reaction was calculated using an extinction coefficient of 9.6 $mM^{-1}$ $cm^{-1}$. The succinate-ferricyanide reductase activity was determined at 420 nm ($\epsilon$ = 1 $mM^{-1}$ $cm^{-1}$) with 20 mM succinate and 200 $\mu$M ferricyanide. (In each case, the concentration of substrate was much greater than the Michaelis constant.) Solution assays were carried out in 50 mM potassium phosphate at pH 7.0 and at 25 °C. We obtained the turnover numbers $k_2^{succ} = 12\ s^{-1}$ and $k_2^{fum} = 450\ s^{-1}$ for FrdAB activity toward succinate oxidation and fumarate reduction, respectively.

Beef heart SQR was isolated from mitochondria by the method of Beginsky and Hatefi (*46*), and pure fractions of soluble SDH were obtained by resolution with perchlorate (*47*).

*Electrochemistry.* Experiments were performed with a mixed buffer system consisting of 10 mM in each of CHES, HEPES, and TAPS (Sigma) containing 0.1 M NaCl as additional supporting electrolyte. Mixtures were titrated with NaOH or HCl to the desired pH at 20 °C. Substrates (fumaric or succinic acid, Fluka 99.5%) were added from 50 mM stock solutions prepared in the same mixed buffers. Polymyxin B sulfate (Sigma), which enhances the adsorption of FrdAB on the electrode, was prepared as a 20 mg/mL stock solution in water.

A pyrolytic graphite edge (PGE) rotating disk working electrode (*31*) (geometric area $A = 0.03\ cm^2$) was used in conjunction with an EG&G model 636 electrode rotator. A platinum wire was used as counter electrode, and a saturated calomel electrode (SCE) in a Luggin sidearm containing 0.1M NaCl was used as reference. All potentials are quoted against the standard hydrogen electrode (SHE), using $E_{SHE} = E_{SCE} + 241$ mV at 20 °C (*48*). The electrochemical cell was thermostated at 20 °C using a Neslab circulator and housed in a Faraday cage. Voltammetry was performed using an Autolab electrochemical analyzer (Eco Chemie, Utrecht, The Netherlands) controlled by GPES software and equipped with analogue scan generator and electrochemical detection (increased sensitivity) modules. For fast-scan experiments, the effects of uncompensated cell resistance were minimized by using the positive-feedback *iR* compensation function of the potentiostat (*49*).

All voltammetric experiments and handling of enzyme solutions were carried out in a glovebox (Vacuum Atmospheres) under a $N_2$ atmosphere ($O_2$ < 3 ppm). Prior to each experiment the PGE electrode was polished with an aqueous slurry of alumina (1 $\mu$m, Buehler) and sonicated thoroughly. For FrdAB, 5 $\mu$L of enzyme stock (approximately 50 $\mu$M) and 10 $\mu$L of polymyxin solution were mixed and applied to the surface of the electrode which was then inserted directly into the cell whose large volume (4 mL) minimized the influence of fumarate formation during slow scans at high potentials. To study substrate-concentration dependences, a single film of FrdAB was used at each pH and transferred into solutions of increasing succinate concentration. For SDH, the enzyme samples were freed of residual ammonium sulfate and perchlorate by diafiltration, using a micro-dialyzer (Spectrum Micro DispoDialyzer 1356021) against a mixed buffer containing 0.5 mM succinate. Aliquots of the enzyme solution were added to the electrolyte (1 mL) to give a final concentration of 1 $\mu$M. Film formation was then initiated by poising the electrode potential at −200 mV for 30 s, the electrode rotating at 100 rpm. After each experiment, the cell solution was retained, and its pH was checked at 20 °C.

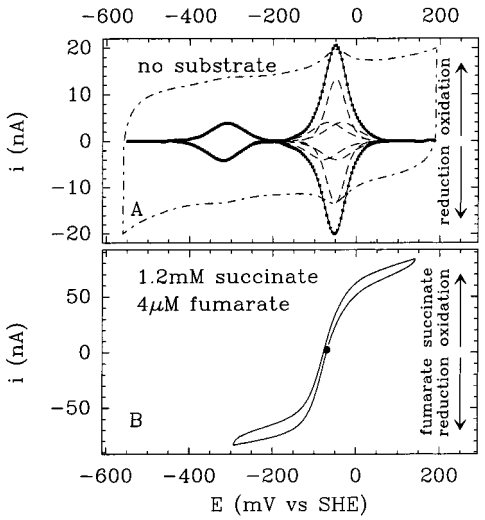


FIGURE 1: (A) Noncatalytic voltammograms obtained for FrdAB adsorbed at a PGE electrode in the absence of substrate. The raw voltammogram (outer dash−dot line) is not to scale. The inset shows the background corrected current (small dots) and deconvoluted data. $[2Fe2S]^{2+/+}$, $E_{m,7} = -35$ mV; $[3Fe4S]^{+/0}$, −67 mV; $[4Fe4S]^{2+/+}$, −310 mV; FAD quinone/hydroquinone: −50 mV (dashed lines for individual contributions and plain lines for their sum). Stationary (non-rotating) electrode, area $A = 0.03\ cm^2$, scan rate $\nu$ = 10 mV/s, temperature $T$ = 20 °C, pH 7. (B) Catalytic wave showing reversible succinate oxidation and fumarate reduction by adsorbed FrdAB in a solution containing succinate and fumarate in concentrations [S] = 1.2 mM and [F] = 4 $\mu$M, respectively. The scan was started from the open circuit potential marked with a filled circle. $\nu$ = 1 mV/s, $T$ = 20 °C, pH 7, electrode rotation rate $\omega$ = 3000 rpm.

The voltammetric data were analyzed using an in-house program. The noncatalytic data were filtered using a Fourier transform (*50*) and corrected for charging current by interpolating the baseline on each side of the voltammetric peaks using a cubic spline procedure (*50*); deconvolution of the signals was then performed by least-squares fitting to the sum of four independent[2] redox transitions. The peaks associated with each center were assumed to have the nernstian shapes given in ref 48 and 55 for the one- and two-electron signals, respectively. Six parameters were simultaneously adjusted: four reduction potentials (three [Fe−S] clusters and the FAD), the disproportionation constant of the FAD ($\kappa$) and the electroactive coverage ($A\Gamma$). The assignment of each one-electron peak to an Fe−S cluster has been done as in ref *32*. The catalytic voltammograms were corrected for charging current by subtracting a second-order polynomial from the wave, such that at the low- and high-potential limits the corrected current was constant (*32*).

## RESULTS AND MODELING

*Noncatalytic Voltammetry.* Figure 1A shows a voltammogram of FrdAB adsorbed at a PGE electrode. In the absence of substrate, sweeping across the potential range

[2] This assumption should be questioned, but the relatively low-intensity noncatalytic peak currents observed for large enzymes adsorbed on an electrode seems to to preclude the investigation of possible cooperativity between the different redox centers. For discussions of these effects in the context of ET in multicentered enzymes, see, e.g., refs 51−54.

produces current peaks due to electron transfer between the electrode and the different redox centers in the enzyme. In the limiting case of an active site undergoing a fully cooperative transfer of $n$ electrons, the peak current varies as $n^2$ and the half-height width varies as $n^{-1}$ (*28*).

In the potential range −600 to +200mV, four signals (pairs of oxidation and reduction peaks) are observed (*31*, *32*): these are the one-electron transitions of the three Fe−S clusters, and the prominent two-electron transition of the FAD (quinone/hydroquinone, −50 mV at pH 7) which clearly exhibits some cooperativity. In Figure 1A, the outer trace is a cyclic voltammogram recorded at pH 7. After subtracting the charging current, the resulting faradaic voltammogram can be deconvoluted to determine the contributions of the individual centers. Integrating the current over half a cycle yields the total number of electrons transferred, and thus the electroactive enzyme coverage—in this experiment, $\Gamma \approx 13$ pmol/cm$^2$.

*Steady-State Catalysis.* Figure 1B shows a voltammogram recorded for an FrdAB film in contact with a solution containing both succinate and fumarate, at concentrations [S] = 1.2 mM and [F] = 4 $\mu$M, respectively. A low scan rate was used ($\nu$ = 1 mV/s) to ensure steady state ($k_2$ for succinate oxidation is low, vide infra).

The resulting voltammogram is a "direct read-out" of the rate of catalysis in either direction as a function of the electrode potential (driving force). At an applied potential ($E$) higher than the fumarate/succinate equilibrium potential ($E_{F/S}$), electrons flow from succinate to electrode via the FAD and Fe−S clusters; the resulting (positive) current is directly proportional to the rate of succinate oxidation. At low potential the net direction of electron flow is reversed; a negative current is now observed that is proportional to the rate of fumarate reduction. The limiting currents at very high or very low potential ($i_{lim}^{succ}$ and $i_{lim}^{fum}$) reflect the maximal rate of turnover in either direction, for given concentration of substrates, when regeneration of the active site by the electrode is not limiting.

The filled circle in Figure 1B indicates the potential of zero net current (or "open circuit potential") at −51 mV. This should correspond to $E_{F/S}$ which can be calculated for any concentration ratio using the Nernst equation and the published value $E^{0'}_{F/S} \approx +20$ mV at 25 °C, pH 7 (*57*); $E_{F/S} = E^{0'}_{F/S} + {}^{RT}/_{2\mathcal{F}} \ln([F]/[S]) = -46$ mV ($\mathcal{F}$ is the Faraday constant, $R$ the gas constant, and $T$ the temperature).

The direction and rate of catalysis depend on the electrode potential and the concentrations of reactants and on the enzyme's intrinsic catalytic bias which is defined as the ratio of the potential-independent first-order rate constants for succinate or fumarate conversion in the enzyme−substrate complex ($k_2^{succ}$ and $k_2^{fum}$). In Figure 1B, $i_{lim}^{succ}/i_{lim}^{fum}$ is approximately 1 for a [S]/[F] ratio of 300, suggesting that FrdAB is significantly biased in the direction of fumarate reduction. However, as explained below, quantitative analysis requires consideration of binding effects.

Figure 2 shows as-measured (panel A) and baseline-subtracted (panel B) cyclic voltammograms for succinate oxidation in fumarate-free solutions at pH 7.5. The experiments have been performed with the same FrdAB film successively transferred to pH-buffered solutions of increasing succinate concentration in the range [S] = 20 $\mu$M to 16 mM. The electrode rotation rate was sufficiently high that

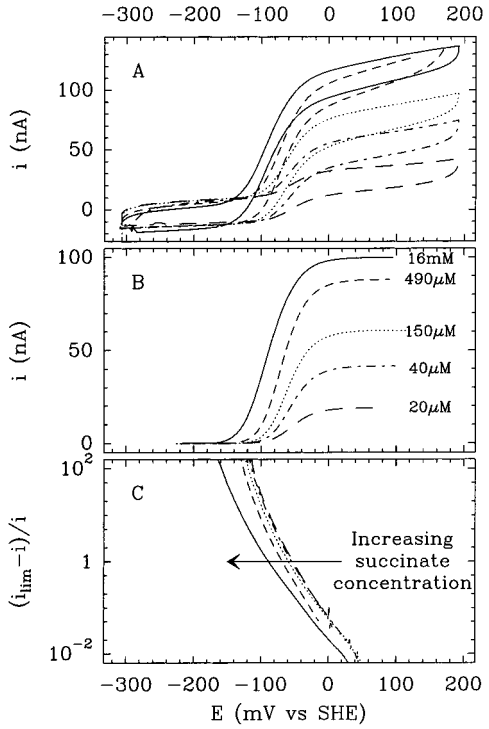


FIGURE 2: Substrate-concentration dependence of catalytic voltammetry for succinate oxidation by FrdAB. Raw catalytic voltammograms (A), baseline subtracted data (B) and semilogarithmic plot of the catalytic waves (C). pH 7.5, scan rate $\nu$ = 1 mV/s, electrode rotation rate $\omega$ = 3000 rpm, temperature $T$ = 20 °C, succinate concentration [S] = 20 $\mu$M to 16 mM (no fumarate).

raising it further produced no noticeable increase in current; thus there is neither substrate depletion nor product accumulation near the interface (*56*). Importantly, in addition to the expected increase in catalytic current as the succinate concentration is raised, the position of the wave shifts to more negative potentials.

A second important feature becomes apparent in the corresponding Heyrovsky-Ilkovich plot shown in Figure 2C. This plot of $\log_{10}[(i_{lim} - i)/i]$ against $E$ is usually used to analyze sigmoidal polarographic waves recorded under steady-state *diffusion-limited* conditions (*58*). For an $n$-electron electrochemical reaction that is reversible (i.e., the Nernst equation is obeyed at all times), the plot is linear with a slope $-n\mathcal{F}/2.3RT$. By contrast, Figure 2C shows a significant upward curvature over the entire range of succinate concentration.

*Derivation of a Potential-Dependent Michaelis−Menten Model.* The first-order rate constant for succinate oxidation by FrdAB can be estimated immediately from the magnitude of the catalytic currents in Figure 2 using

$$\frac{i_{lim}}{2\mathcal{F}A\Gamma} = \frac{k_2^{succ}}{1 + \dfrac{K_m^{succ}}{[S]}} \qquad (2)$$

[The $2\mathcal{F}A\Gamma$ term arises because the current is proportional to the total electroactive coverage ($A\Gamma$) and the fumarate/succinate transformation involves two electrons.] Assuming an electroactive coverage of $A\Gamma \approx 10^{-13}$ mol, $k_2^{succ}$ is of the order of a few (seconds)$^{-1}$; therefore, catalytic oxidation can be described by a Michaelis−Menten (M−M) scheme, in

Scheme 1: Catalytic Cycle for the Oxidation of Succinate by SDH and FrdAB[a]

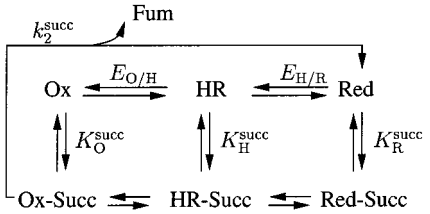


[a] Ox, HR (half-reduced) and Red are used to denote the three redox states of the FAD (quinone, semiquinone and hydroquinone respectively). $E_{O/H}$ and $E_{H/R}$ are the one-electron reduction potentials for the quinone/semiquinone and semiquinone/hydroquinone transformations. The average two-electron reduction potential quinone/hydroquinone is $E_{O/R} = (E_{O/H} + E_{H/R})/2$.

which all binding steps are fast relative to reactions within the enzyme−substrate complex. The limiting current depends on the (surface) concentration of substrate-bound enzyme, which is proportional to $[S]/([S] + K_O^{succ})$, where $K_O^{succ}$ is the dissociation constant from the oxidized active site. Thus $K_O^{succ}$ and $k_2^{succ}$ can be determined from the variation in limiting current with substrate concentration shown in Figure 2B.

To interpret the shapes of the voltammograms and determine the energetics of the catalytic mechanism, we must add the "potential dimension" to the M−M model and incorporate the Nernst equation to relate the populations of the different redox forms of the FAD to the electrode potential ($E$). We consider only the states of the FAD, and assume that the role of the Fe−S clusters is to mediate the electrons. In Scheme 1, $E_{O/H}$ is the reduction potential for the one-electron interconversion between oxidized and half-reduced forms, and $E_{O/R}$ is the average two-electron reduction potential. We get

$$\frac{i}{2\mathcal{F}A\Gamma} = \frac{k_2^{succ}/\left(1 + \frac{K_O^{succ}}{[S]}\right)}{1 + \exp\left[\frac{\mathcal{F}}{RT}(E_{O/H} - E)\right] + \exp\left[\frac{2\mathcal{F}}{RT}(E_{O/R} - E)\right]} \quad (3)$$

by assuming that the current is proportional to the concentration of oxidized, substrate-bound enzyme.[3]

The denominator of eq 3 hides a substrate-concentration dependence: the potentials of the redox transitions are related to their values in a succinate-free solution [$E_{O/R}([S] = 0)$ and $E_{O/H}([S] = 0)$], to the succinate concentration ([S]), and to the dissociation constant from the oxidized, semi-reduced, and reduced forms of the FAD ($K_O^{succ}$, $K_H^{succ}$, and $K_R^{succ}$) according to

$$E_{O/R} = E_{O/R}([S] = 0) + \frac{2.3RT}{2\mathcal{F}} \log_{10} \frac{1 + [S]/K_R^{succ}}{1 + [S]/K_O^{succ}} \quad (4a)$$

$$E_{O/H} = E_{O/H}([S] = 0) + \frac{2.3RT}{\mathcal{F}} \log_{10} \frac{1 + [S]/K_H^{succ}}{1 + [S]/K_O^{succ}} \quad (4b)$$

An equation similar to 4a was used previously to determine the dissociation constants $K_O^{OAA}$ and $K_R^{OAA}$ from the oxaloacetate-concentration-dependent potential of the FAD in FrdAB, measured using noncatalytic voltammetry (*32*).

At high potential, the exponential terms in eq 3 vanish (FAD is fully oxidized), and the current equation reduces to a M−M form, with limiting current current ($i_{lim}$) given by

$$\frac{i_{lim}}{2\mathcal{F}A\Gamma} = \frac{k_2^{succ}}{1 + \frac{K_O^{succ}}{[S]}} \quad (5)$$

From eqs 3 and 5, we obtain the logarithmic transform of the wave,

$$\log_{10}\left(\frac{i_{lim} - i}{i}\right) = \log_{10}\left(\exp\left[\frac{\mathcal{F}}{RT}(E_{O/H} - E)\right] + \exp\left[\frac{2\mathcal{F}}{RT}(E_{O/R} - E)\right]\right) \quad (6)$$

$$\approx \begin{cases} \frac{\mathcal{F}}{2.3RT}(E_{O/H} - E) \text{ at high potential,} \\ \frac{2\mathcal{F}}{2.3RT}(E_{O/R} - E) \text{ at low potential,} \end{cases}$$

which is expected to show a crossover between two limiting behaviors: the plot should be linear at high potential with a slope $-\mathcal{F}/2.3RT$ decade/mV and also linear at lower potential, but with a slope $-2\mathcal{F}/2.3RT$ decade/mV (−58 and −29 mV/decade, respectively, at 20 °C).

*Data Analysis.* Figure 3 demonstrates that the model accounts for both the change in limiting current as a function of succinate concentration (eq 5) and for the waveshape (eq 6).

Figure 3A shows a plot of $i_{lim}$ as a function of $i_{lim}/[S]$ at pH 7.5; this is an Eadie-Hofstee plot, slope $= -K_m^{succ}$ (*59*). The best fit gives $K_m^{succ} = (83 \pm 5)$ $\mu$M for succinate oxidation by FrdAB.

Logarithmic transforms of two catalytic voltammograms are plotted in Figure 3B. The average slopes are $-n_{app}\mathcal{F}/2.3RT$, where $n_{app}$ is an apparent number of electrons greater than one (*31*): this qualitatively conveys the cooperative character of electron transfer at the FAD.[4] As predicted by the model, each plot shows upward curvature and tends toward limiting slopes $-\mathcal{F}/2.3RT$ and $-2\mathcal{F}/2.3RT$ decade/mV at high and low potentials, respectively. Moreover, eq 6 accounts well for the data in the entire potential range (plain lines in Figure 3B), with only two adjustable parameters. For a given substrate concentration and pH, the fit yields values of the FAD reduction potentials, $E_{O/R}$ and $E_{O/H}$, shown as filled and empty squares, respectively.

[3] Applying the Nernst equation, the fraction of FAD in the oxidized form equates to $(1 + \exp[\mathcal{F}/RT(E_{O/H} - E)] + \exp[2\mathcal{F}/RT(E_{O/R} - E)])^{-1}$. This has to be multiplied by $[S]/([S] + K_O^{succ})$ to obtain the fraction of oxidized, succinate-bound enzyme, and then by $k_2^{succ}$ to obtain the turnover number, and by $2\mathcal{F}A\Gamma$ to obtain the catalytic current.

[4] There is a *formal* analogy between the Heyrovsky−Ilkovich plot and the Hill plot used in studies of cooperative binding in allosteric proteins. From the measurement of the saturation ($Y$) as a function of the substrate concentration ([S]), the cooperativity is evidenced in a Hill plot of $\log_{10}(Y/(1 - Y))$ against $\log_{10}([S])$. $Y$ is analogous to the current (which is proportional to the fraction of oxidized enzyme), and $\log_{10}(Y/(1 - Y))$ is analogous to $\log_{10}((i_{lim} - i)/i)$. The average slope of a Hill plot or a Heyrovsky−Ilkovich plot exceeds one when binding or ET, respectively, is a cooperative event.

Table 1: Thermodynamics Properties of FAD in FrdAB Measured at 20 °C from the Analysis of Voltammograms

| pH | $K_m^{succ}$ [a] | $K_O^{succ}$ [b,c] | $K_H^{succ}$ [b,c] | $K_R^{succ}$ [b,c] | $E_{O/R}$ [d,e] | $E_{O/R}$ [c,e] | $E_{O/H}$ [c,e] |
|---|---|---|---|---|---|---|---|
| 7 | | 0.14 | 0.31 | 8 | −50 | −42 | −45 |
| 7.5 | 0.083 ± 0.005 | 0.18 | 0.63 | 9 | −65 | −59 | −66 |
| 8 | 0.130 ± 0.01 | 0.25 | 1.8 | 12 | −80 | −78 | −88 |
| 8.5 | | 0.71 | 6.3 | 16 | −97 | −109 | −103 |
| 9 | | 0.8 | 10 | 11 | −118 | −124 | −110 |
| 9.5 | | 0.8 | nd[f] | 8 | −142 | −141 | nd[f] |

[a] Michaelis constant in mM. From Eadie-Hofstee plots (as in Figure 3A), provided the films were sufficiently stable. [b] Dissociation constants are in mM. Since fitting the data with eq 4 gives the log of the dissociation constants with an error ±0.1, the error on a dissociation constant $K$ is ±0.1 × 2.3 × $K$. [c] From catalytic data. [d] From noncatalytic data. Reproducibility ±3 mV. [e] All potentials correspond to succinate-free FAD, and are in millivolts vs SHE. The good agreement between the values of $E_{O/R}$ obtained from noncatalytic and catalytic data suggests that the error on the latter is lower than 10 mV. The errors on $pK_H^{succ}$ and $E_{O/H}$ are correlated: an error ±0.1 on $pK_H^{succ}$ results in an *additional* error of ±0.1 × 60 mV on $E_{O/H}$. [f] At pH 9.5, the data are too noisy to be fitted with eq 4b, therefore these values could not be determined.

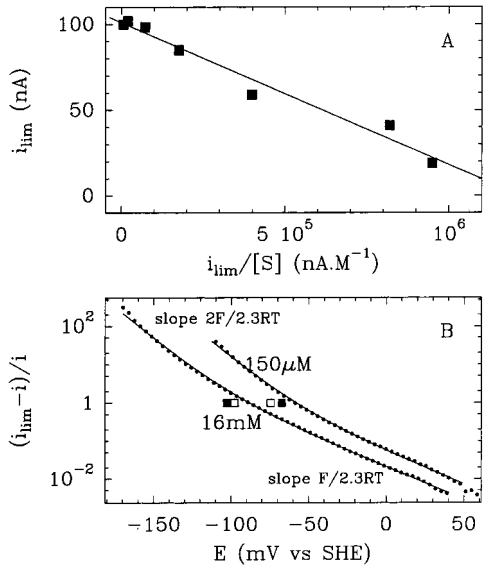


FIGURE 3: Analysis of steady-state catalytic waves for succinate oxidation by FrdAB. (A) Eadie-Hofstee plot to determine $K_m^{succ}$ from the change in limiting current as a function of the substrate concentration (eq 5). Same conditions as in Figure 2. The best fit to a straight line gives $K_m^{succ}$ = (83 ± 5) μM. (B) Heyrovsky−Ilkovich plot of two of the voltammograms plotted in Figure 2 (for [S] = 150 μM and [S] = 16 mM). The small filled circles are the raw data. At each concentration, the fit to eq 6 (plain line) gives the values of $E_{O/R}$ (■) and $E_{O/H}$ (□).

*Thermodynamic Properties of the FAD from Catalytic Voltammetry.* Experiments were conducted at several pHs (7−9.5) for a range of succinate concentrations 20 μM to 50 mM, and in each case, values of $E_{O/R}$ and $E_{O/H}$ were determined from the fits to eq 6. Figure 4 shows that both $E_{O/R}$ and the stability of the semiquinone state (related to $E_{O/H} - E_{O/R}$) depend on pH and succinate concentration.

For each pH, values of $E_{O/R}$([S] = 0), $K_O^{succ}$ and $K_R^{succ}$ were determined by fitting the values $E_{O/R}$ against [S] to eq 4a, then the fit of $E_{O/H}$ to eq 4b gave $E_{O/H}$([S] = 0) and $K_H^{succ}$. The best parameters are reported in Table 1. The most pronounced pH dependence is observed for $K_H^{succ}$ which decreases 30-fold between pH 7 and 9. As found also for SDH (*5*, *60*) the dissociation constants for succinate decrease (binding is enhanced) when the FAD is oxidized.

The pH dependence of the FAD reduction potentials (Table 1) yields the number of protons involved in the redox transformations of the active site. Figure 5 shows that $E_{O/R}$ decreases by about 30 mV/pH unit in the pH range investigated 7−9.5, thus, one proton is transferred for the two-electron reaction, i.e., the active site operates between neutral quinone (FAD) and anionic hydroquinone ($FADH^-$) states. In 1 mM succinate, $E_{O/R}$ shifts by about −25 mV without changing the pH dependences of the redox processes.

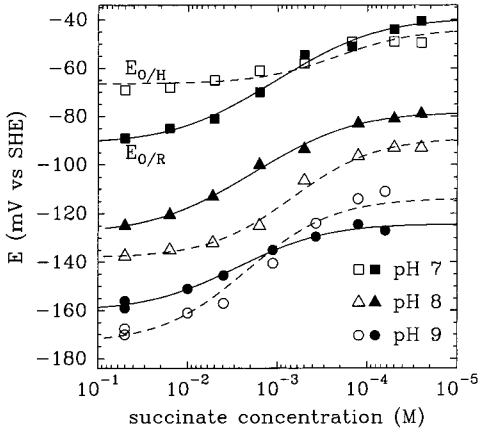


FIGURE 4: Changes, observed for FrdAB, in the two-electron reduction potential of FAD quinone/hydroquinone (filled symbols) and one-electron reduction potential of FAD quinone/semiquinone (empty symbols) as a function of the succinate concentration and for different pHs. These were measured by fitting catalytic voltammograms with eq 6. $T$ = 20 °C. The symbols correspond to pH 7 (squares), 8 (triangles), and 9 (circles). Lines are best fits with eqs 4.

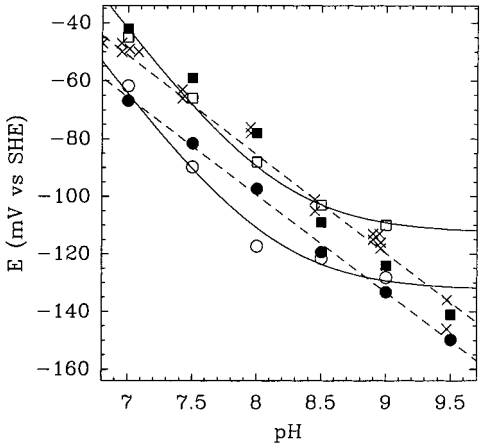


FIGURE 5: pH dependences of FrdAB active site FAD reduction potentials; $E_{O/R}$ (filled symbols) and $E_{O/H}$ (empty symbols) for [S] = 0 (squares) and [S] = 1 mM (circles). Crosses (×) are values of $E_{O/R}$ determined from noncatalytic data at [S] = 0. For $E_{O/R}$, best fits (dashed straight lines) give slopes −34 mV/pH. For $E_{O/H}$ fits to eq 7 (plain lines) give $pK_a$ = 8.15 ± 0.1.

Fitting the pH dependence of $E_{O/H}$ to

$$E_{O/H} = E^{alk}_{O/H} + \frac{2.3RT}{\mathscr{F}}\log_{10}\left(1 + \frac{[H^+]}{K_a}\right) \quad (7)$$

(plain lines in Figure 5), gives $pK_a = 8.15 \pm 0.10$ for the semiquinone form of the flavin.

In support of the above analysis, the values of several parameters determined in two independent ways were compared. With sufficiently stable films, Michaelis constants were determined by Eadie-Hofstee plots yielding values of $K_m^{succ}$, which matched the independently measured $K_O^{succ}$ (Table 1), as expected from eq 5. Additionally, we compared the average two-electron substrate-free potentials of the FAD measured either (i) by analyzing the catalytic wave and extrapolating the concentration dependence of $E_{O/R}$ to zero succinate concentration using eq 4a, or (ii) by deconvoluting the noncatalytic voltammograms recorded in substrate-free solution (Figure 1A). The difference was always less than 10 mV (see Table 1, and compare the filled squares and crosses in Figure 5). The cooperativity of the ET process at zero succinate concentration can be estimated by analyzing the FAD peak in noncatalytic experiments. Fitting the data in Figure 1A at pH 7 yields a disproportionation constant $\kappa = 0.2 \pm 0.1$, therefore $E_{O/H} - E_{O/R} = -22 \pm 8$ mV. By extrapolating catalytic data to zero succinate concentration (Table 1) we obtained $E_{O/H} - E_{O/R} = -3 \pm 20$ mV. Both estimates suggest a significant maximal level of semiquinone (respectively, $20 \pm 5$ and $35 \pm 15\%$) at $E = E_{O/R}$, pH 7, in the absence of substrate.

*Product Inhibition and Estimation of the Catalytic Bias of FrdAB.* From Scheme 2, the limiting current for succinate oxidation ($i_{lim}^{succ}$) in the presence of succinate and fumarate follows M−M kinetics with the apparent $K_m^{succ}$ increased by a factor $(1 + [F]/K_O^{fum})$, where $K_O^{fum}$ is the fumarate dissociation constant for oxidized FAD. Symmetrical reasoning holds for fumarate reduction inhibition by succinate at low potential so that:

$$\frac{i_{lim}^{succ}}{2\mathscr{F}A\Gamma} = \frac{k_2^{succ}}{1 + \frac{K_m^{succ}}{[S]}\left(1 + \frac{[F]}{K_O^{fum}}\right)} \quad (8a)$$

$$\frac{i_{lim}^{fum}}{2\mathscr{F}A\Gamma} = \frac{-k_2^{fum}}{1 + \frac{K_m^{fum}}{[F]}\left(1 + \frac{[S]}{K_R^{succ}}\right)} \quad (8b)$$

Four parameters ($K_m^{succ}$, $K_m^{fum}$, $K_O^{fum}$, and $K_R^{succ}$) are required to estimate the catalytic bias of FrdAB from eqs 8 and the experiment plotted in Figure 1B. At pH 7, $K_m^{fum} = 160$ $\mu$M (*31*), $K_m^{succ} = 140$ $\mu$M and $K_R^{succ} = 8$ mM (Table 1). The remaining parameter is $K_O^{fum}$, which is likely to be much higher than the fumarate concentration used ([F] = 4 $\mu$M). The ratio of limiting current therefore simplifies to[5]

$$\frac{i_{lim}^{succ}}{i_{lim}^{fum}} \approx -\frac{k_2^{succ}K_m^{fum}}{k_2^{fum}[F]} \quad (9)$$

The limiting currents for succinate oxidation and fumarate reduction are roughly equal to each other under the conditions of Figure 1B. Equation 9 gives $k_2^{fum}/k_2^{succ} \approx 40$, while a similar value (approximately 37) was obtained in solution assays at 25 °C, pH 7, based on methyl viologen or ferricyanide as the electron partner (Experimental Section). Using the value $k_2^{fum} \approx 840$ s$^{-1}$ obtained for WT FrdAB adsorbed onto an electrode (*31*), we obtain $k_2^{succ} \approx 20$ s$^{-1}$ for succinate oxidation at pH 7.

Scheme 2: Product Inhibition of Succinate Oxidation at High Electrode Potential (top) and Fumarate Reduction at Low Potential (bottom)

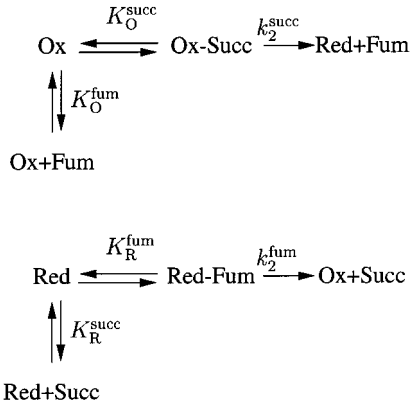


*Fast-Scan Voltammetry in the Presence of Substrate.* Fast-scan voltammetry provides another way to study the FAD cofactor during catalysis (*38*). Figure 6 shows how the FAD oxidation and reduction peak positions vary with scan rate in the absence of succinate (empty symbols). Because (i) the two electrons transfer cooperatively (*55*) (see Figure 1A) and (ii) ET to the FAD is fast, the signal is prominent and could be tracked over 4 orders of magnitude in scan rate ($\nu$ = 10 mV/s to 100 V/s). By analyzing the position of peaks as a function of scan rate, information on the rates of interfacial ET and coupled chemical processes can be obtained (*30*, *32*).

When succinate is bound, the plot of FAD peak positions against $\nu$ (filled symbols in Figure 6) commences at a scan rate that is high enough to outrun catalysis, i.e., allowing the electrons to be re-injected before transformation of the $FAD_{Ox}$−succinate enzyme−substrate complex. The scans in the presence of substrate were started from a reductive poise, in 50 mM succinate at pH 7. Since $K_R^{succ} = 8$ mM (Table 1), the active site is 86% saturated. As seen in Figure 6, the average peak position of the FAD at pH 7, [S] = 50 mM is $E_{O/R} = -80$ mV vs SHE. This value matches well that determined from the waveshape in the same conditions ($E_{O/R} \approx -88$ mV, Figure 4). The shift of about −31 mV seen in Figure 6 is smaller than expected from Figure 4, where 50 mM succinate causes a shift of nearly −50 mV. This discrepancy is likely to arise to the greater error in $E_{O/R}$ determined from catalytic data at very low concentration of succinate (due to the small currents which are then mea-

[5] Since the fumarate concentration is very low, it should not inhibit succinate oxidation. Moreover, the succinate concentration is much higher than $K_O^{succ}$, so the right-hand side of eq 8a reduces to $k_2^{succ}$. Regarding the limiting reductive current, the succinate concentration is much lower than $K_R^{succ}$ —too low to inhibit fumarate reduction. With the fumarate concentration being lower than $K_m^{fum}$, the denominator of eq 8b approximates to $K_m^{fum}/[F]$.

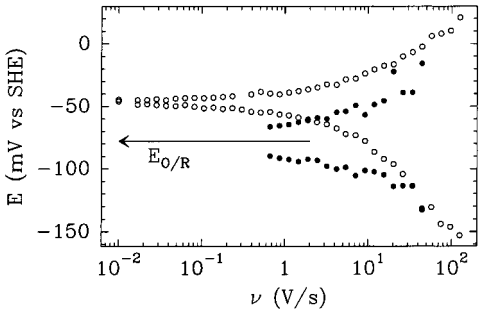


FIGURE 6: Fast-scan voltammetry of FrdAB without succinate (○) and with 50 mM succinate (●) at pH 7. The prominent high-potential (FAD) peak position is plotted as a function of the scan rate. The arrow marks the value of $E_{O/R}$ in the presence of 50 mM succinate. When succinate was present, the cyclic voltammograms were recorded between −610 and +240 mV, after 5 s equilibration at low potential.

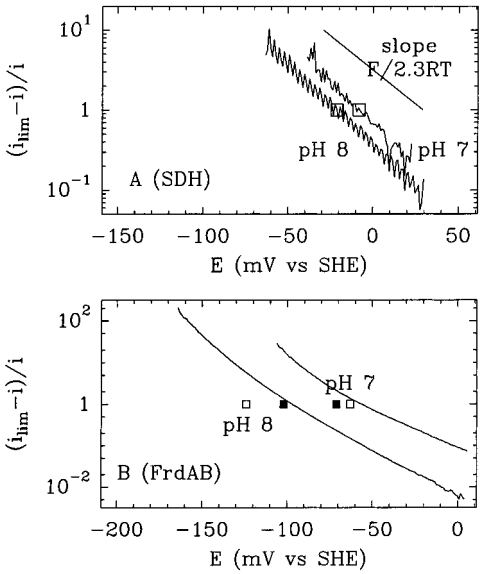


FIGURE 7: Comparison between SDH (A) and FrdAB (B): pH dependence of $E_{O/H}$. pH 7 and 8, [S] = 1.5 mM (FrdAB) and [S] = 0.8 mM (SDH). As in Figure 3, the sets of two squares mark the values of $E_{O/R}$ (■) and $E_{O/H}$ (□). In plot A, $E_{O/R}$ cannot be determined from the analysis of the waveshape with eq 10. $T = 20$ °C, $\omega = 1000$ rpm (SDH) and 3000 rpm (FrdAB), $\nu = 10$ mV/s (SDH) and 1 mV/s (FrdAB).

sured). Under fast scan conditions, in the presence of substrate, we did not notice any change in the stoichiometry of the FAD signal compared to the one-electron [4Fe-4S] couple.

*Comparison with SDH.* Figures 7 and 8 emphasize the differences in catalytic energetics between SDH and FrdAB. In both figures, the upper plots (Figures 7A and 8A) are the logarithmic transforms of catalytic voltammograms for SDH adsorbed at PGE, whereas the lower plots (Figures 7B and 8B) correspond to catalysis by FrdAB under the same conditions. For reasons that remain unclear, SDH does not give a high electroactive coverage at PGE (nonturnover signals have not been reliably detected) and the films are unstable (*33*−*36*). Even so, the data are well-defined enough to draw comparative insights.

Two catalytic voltammograms for succinate oxidation by SDH are plotted in Figure 7, differing only in pH. The waveshape is not distinguishable from a line of slope $-\mathcal{F}/2.3RT$ decade/mV that is expected from the above M−M model if the semiquinone is stable (i.e., $E_{O/H} \gg E_{O/R}$). In this case, eq 6 reduces to[6]

$$\log_{10}\left(\frac{i_{lim}-i}{i}\right) \approx \frac{\mathcal{F}}{2.3RT}(E_{O/H}-E) \qquad (10)$$

and the logarithmic plot intercepts the line for $(i_{lim} - i)/i = 1$ at $E = E_{O/H}$, i.e., the mid-wave potential is $E_{O/H}$ (shown as empty squares in Figure 7A). Note that the position of the wave provides no information on $E_{O/R}$. The one-electron shape of the wave is unambiguous evidence that the semiquinone form of FAD in SDH is stable over quite a large range of potential although the conclusion that the mid-wave potential equals $E_{O/H}$ (eq 10) is based on the assumption that binding of succinate is a rapidly established equilibrium.[7]

As seen in Figure 7A, the value of $E_{O/H}$ as determined from the waveshape with eq 10 decreases by approximatively 10 mV when the pH is increased from 7 to 8. This pH dependence of the mid-wave potential has been reported previously (*34*−*36*) but may now be interpreted. For FrdAB, the −60 mV/pH dependence of $E_{O/H}$ (Figure 7B) shows that the FAD is protonated upon reduction to the semiquinone state; by contrast, for SDH, the very small pH dependence of $E_{O/H}$ now shows that the semiquinone form is anionic at neutral pH, consistent with EPR results (*61*).

In the case of FrdAB at pH 9, $E_{O/H}$ shifts by about −55 mV when the succinate concentration is raised from 50 μM to 50 mM (empty squares in Figure 8B). This must result from the higher affinity of succinate for the oxidized FAD than for the semiquinone form under alkaline conditions (Table 1). A clear contrast is now evident with SDH, where $E_{O/H}$ is hardly sensitive to succinate concentration (Figure 8A). According to eq 4b this suggests that in SDH, binding of succinate at high pH does not depend on whether the FAD is in the quinone or semiquinone state.

## DISCUSSION

In classical enzyme kinetics, turnover is measured as a function of the concentrations of various reactants (substrate, protons, inhibitors) and a plausible mechanism is derived. Such studies rely on the relationship between the concentration of reactants and their microscopic rates of binding, which affect the measurable rate of turnover. PFV adds the "potential dimension" to this investigation since rates of redox processes depend on the electrode potential. This strong dependence (exponential at low driving force, as opposed to a linear dependence of binding rate on species concentration) enables the rates of redox reactions to be tuned

[6] Using $\kappa = \exp(^{2\mathcal{F}}/_{RT}(E_{O/H} - E_{O/R}))$, eq 6 reads:

$$\log_{10}\left(\frac{i_{lim}-i}{i}\right) = \log_{10}\left(\sqrt{\kappa}\exp\left[\frac{\mathcal{F}}{RT}(E_{O/R}-E)\right] + \exp\left[\frac{2\mathcal{F}}{RT}(E_{O/R}-E)\right]\right) \qquad (11)$$

If the semiquinone is very stable ($\kappa$ large), the first term is much greater than the second (except at extremely low potential, where hardly any current can be measured), and eq 11 simplifies into eq 10.

[7] In contrast with FrdAB, this hypothesis is questionable in the case of SDH since the generally accepted physiological role of the latter enzyme is to catalyze succinate oxidation. Just as in the case of Briggs−Haldane kinetics where the Michaelis constant is not a true dissociation constant, the one-electron mid-wave potential for succinate oxidation by SDH may have to be interpreted as an "apparent" $E_{O/H}$.

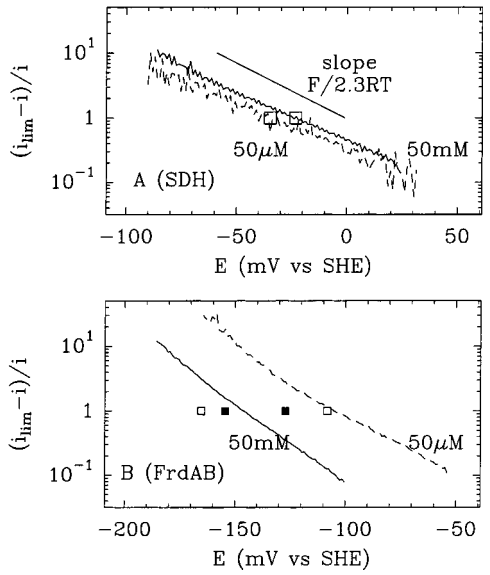


FIGURE 8: Comparison between SDH (A) and FrdAB (B): succinate-concentration dependence of $E_{O/H}$. [S] = 50 $\mu$M (dashed lines) and 50 mM (plain lines). As in Figures 3 and 7, the squares mark the values of $E_{O/R}$ (■) and $E_{O/H}$ (□). $T$ = 20 °C, $\omega$ = 1000 rpm (SDH) and 3000 rpm (FrdAB), $\nu$ = 10 mV/s (SDH) and 1 mV/s (FrdAB).

over orders of magnitude, and makes PFV a potentially powerful method to investigate the catalytic properties of complex multicentered redox enzymes (*28*, *31*−*38*, *40*, *62*).

*FrdAB.* FrdAB, the principal subject of the present study, gives a stable electrochemical response when it is adsorbed onto a graphite electrode. First, we note that the enzyme is firmly biased to operate in the direction of fumarate reduction (Figure 1B), with succinate oxidation being slow.[8] This proves to be a valuable asset in our study of the electrokinetics. The noncatalytic signal (i.e., in the absence of substrate) is easily deconvoluted to measure the reduction potentials of the FAD and the Fe−S clusters (Figure 1A). Due to the cooperativity of the two one-electron transfers, the FAD moiety is easily distinguished as a prominent peak; this provides an alternative to optical or EPR titrations to determine its redox properties and observe its reactions. The two-electron reduction potential of the FAD can even be measured from the peak positions in the presence of substrate, provided the scan rate is high enough to outrun catalysis (*38*). The shift in the FAD noncatalytic signal to low potential when succinate is present (Figure 6) mirrors the shift in the catalytic wave when the concentration of succinate is raised (Figure 2B). As a specific example, Figure 6 shows that at pH 7, [S] = 50 mM, the 2-electron potential of the FAD moves to −80 mV vs SHE. The good agreement with the value of $E_{O/R}$ obtained by analyzing catalytic data ($E_{O/R} \approx -88$ mV at pH 7, [S] = 50 mM, Figure 4) fully supports the model developed here in which the catalytic waveshape is linked to the FAD reduction potentials.

According to eq 6, the semilogarithmic transform of the catalytic wave (the Heyrovsky-Ilkovich plot) reveals a crossover between two limiting behaviors. As indeed confirmed by Figure 2C, the catalytic current as a function of the potential follows a sigmoidal increase with a two- or one-electron shape at low or high driving force, respectively. This can be understood in the following simple terms. According to our hypothesis of rapidly established equilibrium among the different states shown in Scheme 1, the rates of ET and binding are all greater than that for transformation of the enzyme−substrate complex. (i) *At low potential*, reduced FAD accumulates: its oxidation at the electrode appears as a cooperative two-electron reaction because upon formation of the semiquinone form, the second electron is removed spontaneously. (ii) *At higher potential*, the semiquinone form becomes more prevalent, and the waveshape now reflects the further *one*-electron oxidation necessary for turnover. (iii) *At very high potential*, the fully oxidized form of the FAD predominates, and turnover is now limited by the transformation of the $FAD_{Ox}$−succinate complex, the rate of which is potential-independent; the catalytic current thus reaches a plateau.

The model developed here is the electrochemical counterpart of Michaelis−Menten kinetics. We have assumed that catalysis proceeds via hydride transfer between the succinate and FAD. This has the slowest rate constant in the entire sequence of events,[9] over the whole potential range, and ensures that the other processes are always at equilibrium. Consequently, turnover is proportional to the level of fully oxidized (quinone) FAD that can be maintained by the electrode potential. The model would not apply if turnover were limited by ET between electrode and FAD; were this to be the case, the wave would broaden at high driving force (*56*) whereas the limiting slope of the logarithmic transform does not decrease below the nernstian limit of $-\mathcal{F}/2.3RT$ decade/mV (Figure 3B).

Strictly speaking, the net unimolecular rate constant $k_2^{succ}$ that we interpreted as the rate of succinate oxidation in the enzyme−substrate complex could instead be for fumarate release. That this is not the case is shown by fast-scan PFV. If fumarate release were rate limiting, the "faradaic capacity" of the active site, evidenced in the shape of the FAD component of the signal, should increase to four electrons (the $FAD_{Red}$-fumarate enzyme−substrate complex could be further oxidized before the scan is reversed). This change should be easily quantified using the low-potential [4Fe-4S] one-electron signal as a one-electron reference (Figure 1A). Apart from the shift in potential, there was no change in the stoichiometry of the noncatalytic voltammograms recorded at high scan rate in the presence of succinate; this shows that the transformation of the $FAD_{Ox}$-succinate complex into $FAD_{Red}$-fumarate is slower than the release of fumarate.

Importantly, while the cooperativity of the two one-electron transfers at the FAD depends on the pH and succinate concentration, the semiquinone has a significant stability across the whole experimental range (pH = 7−9.5, [S] = 0−50 mM): $E_{O/H} - E_{O/R}$ ranges between −20 and +25 mV (Figure 4); therefore, under turnover conditions, the maximum percentage of semiquinone (at $E = E_{O/R}$) is

[8] The pH dependence of the limiting current for [S] = 50 mM (data not shown) is as expected for a reaction whose rate depends on the basic form of an acid of p$K_a$ = 6.8 ± 0.2. Thus, $k_2^{succ}$ increases less than 2-fold between pH 7 and 9.

[9] Accordingly, the oxidation of perdeuteriosuccinate by SDH is significantly slower than that of succinate, whereas deuteration of fumarate has no observable effect (see ref *35* and references therein). In the case of FrdAB, a large decrease in fumarate reduction activity results upon substitution of $H_2O$ by $D_2O$ (unpublished results).

20−50%. In the absence of substrate, at pH 7, analysis of noncatalytic experiments (the shape of the FAD peak) and extrapolation of catalytic data to zero succinate concentration both suggest that the level of semiquinone at $E = E_{O/R}$ is about 25%. This contrasts with the previous EPR investigation according to which no significant radical signals were observed at 165 K after room-temperature solution titration, and it was concluded that the maximum semiquinone level must be <2% (*32*). The reason for this discrepancy is unclear; however, from the literature, it appears that the stability of the FAD radical in QFR may vary from one preparation to another, and be sensitive to such factors as the presence of the membrane anchor domain (FrdCD) and mutations thereof (*63*, *64*).

The catalytic cycle of succinate oxidation consists of (i) oxidation of the FAD and binding of succinate, and (ii) subsequent oxidation of bound succinate and reduction of the FAD. The only quantity we measure regarding the latter step is its rate, $k_2^{succ}$, and this is also possible with solution assays. However, PFV reveals the thermodynamic properties of the FAD during the reoxidation half-cycle, which is *not* rate limiting during solution assays with oxidizing dyes. Discrete redox states of the FAD can be probed by PFV because it is possible to tune the electrode potential to influence their levels during turnover. From the direct measurement of the FAD reduction potentials as a function of the succinate concentration and pH, we were able to determine the succinate-enzyme dissociation constants for the three redox states of the FAD (Table 1) and the succinate-concentration independent acidity constant of the semiquinone ($pK_a = 8.15 \pm 0.10$). With respect to the model flavin 8α-*N*-imidazolylriboflavin (*65*), the enzyme environment raises the $pK_a$ of the radical by over 1 pH unit. These thermodynamic properties of the FAD are relevant to the catalytic cycle, regarding the protonation and binding states of the FAD intermediates.

During the catalytic cycle of FrdAB, the two-electron reoxidation of the anionic FAD hydroquinone is associated with the loss of one proton. The −60 mV/pH dependence for $E_{O/H}$ below pH 8 (Figure 5) shows that this proton is lost during the one-electron reoxidation of the semiquinone to the quinone. The semiquinone is therefore neutral, and most likely protonated at N5. This contrasts with the finding that 8α-($N^3$-histidyl) covalently bound flavins generally give anionic semiquinone radicals (*61*, *66*).

The data in Table 1 show that at neutral pH, the dissociation constant for the FrdAB enzyme−succinate complex containing reduced FAD is very high, whereas those for the semiquinone and the quinone forms are low (and equal to $K_m^{succ}$) (Table 1). Therefore, unless [S] ≫ 1 mM (for $K_R^{succ} \gg [S] \gg K_m^{succ}$), binding of succinate must occur during the catalytic cycle *after* the hydroquinone is oxidized, i.e., to semiquinone (or quinone) state. In solution assays with high-potential dyes, or in voltammetric measurements on the limiting current plateau, the reoxidation may be so fast that binding could occur later, i.e., to the oxidized form, but not to the reduced form since this is not favored from a thermodynamic viewpoint. However, determining the sequence of binding events occurring in vivo would require to take into account all the dicarboxylates which compete for binding to the active site.

*SDH.* With SDH, a clear and reproducible noncatalytic signal has not so far been detected. This may largely be due to our inability to obtain a sizable coverage. Furthermore, the FAD will not be conspicuous unless the two one-electron transfers show reasonable cooperativity. That the latter is unlikely is evidenced by the fact that the catalytic current can be well fitted to a one-electron sigmoid (Figures 7A and 8A). In view of the model described, this implies that the semiquinone form of the FAD is stable over quite a large potential range, the oxidation of the semiquinone to the quinone being the step revealed in the one-electron wave-shape. In this respect (and like QFR, see above), EPR investigations (in the absence of substrate) have given conflicting results [the maximal percentage of FAD semiquinone measured by EPR ranges from 7% (*67*) to 70% (*61*, *68*)]. Despite this, the measurement of $E_{O/R}$ in SDH from EPR (*67*) is consistent with results from reductive reactivation experiments (*69*). Our previous hypothesis that the attenuation of fumarate reduction at low potential is due to reduction of the FAD (*34*) is not in conflict with the present work: this was modeled as a two-electron switch, but this may well appear at the average two-electron reduction potential of the FAD if the unimolecular rate constant for fumarate reduction ($k_2^{fum}$) depends on the ratio of oxidized to reduced flavin, this quantity being independent of the stability of the semiquinone.

In contrast with FrdAB, reoxidation of the hydroquinone in SDH is thought to involve two protons (*34*, *36*, *67*, *70*) while the present observations suggest that no proton is released during oxidation of the anionic semiquinone. Williamson et al. demonstrated that the interpretation of the pH-dependent reduction potentials of synthetic 8α-*N*-imidazolylriboflavin has to take into account the protonation of the imidazole ring and of the N1, N3, and N5 positions on the isoalloxazine ring (*65*). In flavoenzymes, this could be further complicated by the protonation of nearby amino acid residues and solvent water, and makes doubtful the interpretation of any potentiometric data in the absence of reliable complementary spectroscopic evidence.

## CONCLUDING REMARKS

We have shown previously the SDH activity for fumarate reduction shuts down partly below a certain potential (above a certain driving force) (*33*−*36*, *41*). Such behavior may be widespread for enzymes exhibiting multiple oxidation levels, as evidenced further in our recent report of the catalytic activity of DMSO reductase from *E. coli* (*62*). Just as most enzymes function in vivo at substrate concentrations lower than $K_m$, they are unlikely to be subjected to extremes of electrochemical driving force, dictated by the reduction potential and concentrations of the physiological, membrane-associated electron donor or acceptor. In the case of QFR, the physiologically relevant driving force is given by $E^{0'}_{MQ/MQH_2} + {}^{RT}/_{2\mathcal{F}}\ln{}^{[MQ]}/_{[MQH2]}$. With $E^{0'}_{MQ/MQH_2} = -75$ mV at pH 7; therefore, a 400-fold excess of menaquinone over menaquinol would be required for the activity to lie on the activity plateau at 0 mV (Figure 2B). The physiologically most important region of potential is certainly the *reversible* region (around the reduction potential of the electron partner) that PFV is able to investigate precisely. The potential dependence revealed by our studies is therefore not only a

controllable parameter useful in mechanistic studies, but also a physiologically relevant quantity that should be explored as a possible basis for metabolic regulation.

Determining which amino acid residues are responsible for the differences in the electrocatalytic properties of FrdAB and SDH is an interesting and important task. The distinction is not trivial since even in a single organism, QFR is expressed under anaerobic conditions and SQR under aerobic conditions. This occurs not only in *E. coli*: as a striking example, the maturation of the larvae of the liver fluke *Fasciola hepatica* involves moving from a sheep's lungs to its liver; concomitant with the change from aerobic to anaerobic conditions, the mature fluke stops using SQR and synthesizes QFR as a separate gene product to use fumarate as a terminal oxidant instead of oxygen (*71*). Microorganisms may have evolved separate genes for succinate oxidation and fumarate reduction to obtain directional specificity (to improve the catalytic bias), and not only to speed up the turnover rate.

## ACKNOWLEDGMENT

We thank Sean Elliot, Raúl Camba Acosta, Hendrik A. Heering, Lars C. Jeuken, Anne K. Jones, and Tomoko Ohnishi for fruitful discussions, and Bruce Cochran for assistance in preparing SDH.

## REFERENCES

1. Ohnishi, T., Moser, C. C., Page, C. C., Dutton, P. L., and Yano, T. (2000) *Structure 8*, R23−R32.
2. Ackrell, B. A. C. (2000) *FEBS Lett. 466*, 1−5.
3. Hägerhäll, C. (1997) *Biochim. Biophys. Acta 1320*, 107−141.
4. Gennis, R. B., and Stewart, V. (1996) in *Respiration in E. coli and Salmonella, cellular and molecular biology* (Neidhardt, F., Ed.) Vol. I, chapter 17, pp 217−261, ASM Press, Washington.
5. Ackrell, B. A. C., Johnson, M. K., Gunsalus, R. P., and Cecchini, G. (1992) Structure and function of succinate dehydrogenase and fumarate reductase. In *Chemistry and Biochemistry of flavoenzymes* (Müller, F., Ed.) Vol. III, Chapter 7, pp 229−297, CRC Press, Inc.
6. Maklashina, E., Berthold, D. A., and Cecchini, G. (1998) *J. Bacteriol. 180*, 5989−5996.
7. Guest, J. R. (1981) *J. Gen. Microbiol. 122*, 171−179.
8. Iverson, T. M., Luna-Chavez, C., Cecchini, G., and Rees, D. C. (1999) *Science 284*, 1961−1966.
9. Iverson, T. M., Luna-Chavez, C., Schröder, I., Cecchini, G., and Rees, D. C. (2000) *Curr. Opin. Struct. Biol. 10*, 448−455.
10. Lancaster, C. R. D., Kröger, A., Auer, M., and Michel, H. (1999) *Nature 402*, 377−385.
11. Lancaster, C. R. D., and Kröger, A. (2000) *Biochim. Biophys. Acta 1459*, 422−431.
12. Lancaster, C. R. D., Gross, R., and Simon, J. (2001) *Eur. J. Biochem. 268*, 1820−1827.
13. Leys, D., Tsapin, A. S., Nealson, K. H., Meyer, T. E., Cusanovich, M. A., and Beeumen, J. J. V. (1999) *Nat. Struct. Biol. 6*, 1113−1117.
14. Taylor, P., Pealing, S. L., Reid, G. A., Chapman, S. K., and Walkinshaw, M. D. (1999) *Nat. Struct. Biol. 6*, 1108−1112.
15. Bamford, V., Dobbin, P. S., Richardson, D. J., and Hemmings, A. M. (1999) *Nat. Struct. Biol. 6*, 1104−1107.
16. Mattevi, A., Tedeschi, G., Bacchella, L., Coda, A., Negri, A., and Ronchi, S. (1999) *Structure 7*, 745−756.
17. Reid, G. A., Miles, C. S., Moysey, R. K., Pankhurst, K. L., and Chapman, S. K. (2000) *Biochim. Biophys. Acta 1459*, 310−315.
18. Doherty, M. K., Pealing, S. L., Miles, C. S., Moysey, R. K., Taylor, P., Walkinshaw, M. D., Reid, G. A., and Chapman, S. K. (2000) *Biochemistry 39*, 10695−10701.
19. Tedeschi, G., Ronchi, S., Simonic, T., Treu, C., Mattevi, A., and Negri, A. (2001) *Biochemistry 40*, 4738−4744.
20. Fraaije, M. W., van den Heuvel, R. H. H., van Berkel, W. J. H., and Mattevi, A. (1999) *J. Biol. Chem. 274*, 35514−35520.
21. Mewies, M., McIntire, W. S., and Scrutton, N. S. (1998) *Protein Sci. 7*, 7−20.
22. Stankovich, M. T. (1991) Redox properties of flavins and flavoproteins. In *Chemistry and Biochemistry of flavoenzymes* (Müller, F., Ed.) Vol. I, Chapter 18, pp 401−425, CRC Press, Inc.
23. Tegoni, M., Janot, J. M., and Labeyrie, F. (1986) *Eur. J. Biochem. 155*, 491−503.
24. Harris, C. M., Sanders, S. A., and Massey, V. (1999) *J. Biol. Chem. 274*, 4561−4569.
25. Murataliev, M. B., and Feyereisen, R. (2000) *Biochemistry 39*, 12699−12707.
26. Pollegioni, L., Porrini, D., Molla, G., and Pilone, M. S. (2000) *Eur. J. Biochem. 267*, 6624−6632.
27. Pellett, J. D., Sabaj, K. M., Stephens, A. W., Bell, A. F., Wu, J. Q., Tonge, P. J., and Stankovich, M. T. (2000) *Biochemistry 39*, 13982−13992.
28. Armstrong, F. A., Heering, H. A., and Hirst, J. (1997) *Chem. Soc. Rev. 26*, 169−179.
29. Armstrong, F. A., and Wilson, G. S. (2000) *Electrochim. Acta 45*, 2623−2645.
30. Chen, K., Hirst, J., Camba, R., Bonagura, C. A., Stout, C. D., Burgess, B. K., and Armstrong, F. A. (2000) *Nature 405*, 814−817.
31. Sucheta, A., Cammack, R., Weiner, J., and Armstrong, F. A. (1993) *Biochemistry 32*, 5455−5465.
32. Heering, H. A., Weiner, J. H., and Armstrong, F. A. (1997) *J. Am. Chem. Soc. 119*, 11628−11638.
33. Sucheta, A., Ackrell, B. A. C., Cochran, B., and Armstrong, F. A. (1992) *Nature 356*, 361−362.
34. Hirst, J., Sucheta, A., Ackrell, B. A. C., and Armstrong, F. A. (1996) *J. Am. Chem. Soc. 118*, 5031−5038.
35. Hirst, J., Ackrell, B. A. C., and Armstrong, F. A. (1997) *J. Am. Chem. Soc. 119*, 7434−7439.
36. Pershad, H. R., Hirst, J., Cochran, B., Ackrell, B. A. C., and Armstrong, F. A. (1999) *Biochim. Biophys. Acta 1412*, 262−272.
37. Turner, K. L., Doherty, M. K., Heering, H. A., Armstrong, F. A., Reid, G. A., and Chapman, S. K. (1999) *Biochemistry 38*, 3302−3309.
38. Jones, A. K., Camba, R., Reid, G. A., Chapman, S. K., and Armstrong, F. A. (2000) *J. Am. Chem. Soc. 122*, 6494−6495.
39. Dobbin, P. S., Butt, J. N., Powell, A. K., Reid, G. A., Richardson, D. J. (1999) *Biochem. J. 342*, 439−448.
40. Butt, J. N., Thornton, J., Richardson, D. J., and Dobbin, P. S. (2000) *Biophys. J. 78*, 1001−1009.
41. Ackrell, B. A. C., Armstrong, F. A., Cochran, B., Sucheta, A., and Yu, T. (1993) *FEBS Lett. 326*, 92−94.
42. Jones, A. K., Chapman, S. K., and Armstrong, F. A. Unpublished results.
43. Westenberg, D. J., Gunsalus, R. P., Ackrell, B. A. C., Sices, H., and Cecchini, G. (1993) *J. Biol. Chem. 268*, 815−822.
44. Blaut, M. K., Whittaker, K., Valdovinos, A., Ackrell, B. A. C., Gunsalus, R. P., and Cecchini, G. (1989) *J. Biol. Chem. 264*, 13599−13604.
45. Sambrook, J., Fritsh, E. F., and Maniatis, T. (1989) *Molecular Cloning: a laboratory manual*, Cold Spring Harbor Laboratory, Cold Spring Harbor, NY.
46. Beginsky, M. L., and Hatefi, Y. (1969) *J. Biol. Chem. 244*, 5313−5319.
47. Davis, K. A., and Hatefi, Y. (1971) *Biochemistry 10*, 2509−2516.
48. Bard, A. J., and Faulkner, L. R. (1980) *Electrochemical methods. Fundamental and applications*, John Wiley & Sons, Inc., New York.
49. Britz, D. (1978) *J. Electroanal. Chem. 88*, 309−352.

50. Press, W. H., Teukolsky, S. A., Vetterling, W. T., and Flannery, B. P. (1999) *Numerical Recipes in Fortran 77*, 2nd ed., Cambridge University Press, New York.
51. Bertrand, P., Dole, F., Asso, M., and Guigliarelli, B. (2000) *J. Biol. Inorg. Chem. 5*, 682−691.
52. Guigliarelli, B., and Bertrand, P. (1999) *Adv. Inorg. Chem. 47*, 421−497.
53. Louro, R. O., Catarino, T., Turner, D. L., Piçarra-Pereira, M. A., Pacheco, I., LeGall, J., and Xavier, A. V. (1998) *Biochemistry 37*, 15808−15815.
54. Louro, R. O., Catarino, T., LeGall, J., and Xavier, A. V. (1997) *J. Biol. Inorg. Chem. 2*, 488−491.
55. Plichon, V., and Laviron, E. (1976) *J. Electroanal. Chem. 71*, 143−156.
56. Heering, H. A., Hirst, J., and Armstrong, F. A. (1998) *J. Phys. Chem. B 102*, 6889−6902.
57. Clark, W. M. (1960) *Oxidation−reduction potentials of organic systems*, Baillière, Tindal & Cos Ltd., London.
58. Bond, A. M. (1980) *Modern polarographic methods in analytical electrochemistry*, Marcel Dekker, Inc.
59. Cornish-Bowden, A. (1995) *Fundamental of enzyme kinetics*, Portland Press.
60. Kotlyar, A. B., and Vinogradov, A. D. (1984) *Biochim. Biophys. Acta 784*, 24−34.
61. Ackrell, B. A. C., McIntire, W., Edmondson, D. E., and Kearney, E. B. (1982) The semiquinone form of succinate dehydrogenase and other 8α-substituted flavoenzymes. In *Flavins and Flavoproteins* (Massey, V., and Williams, C. H., Eds.) Chapter 80, pp 488−491, Elsevier North-Holland, Inc.
62. Heffron, K., Léger, C., Rothery, R. A., Weiner, J. H., and Armstrong, F. A. (2001) *Biochemistry 40*, 3117−3126.
63. Weiner, J. H., Cammack R., Cole S. T., Condon C., Honoré N., Lemire B. D., and Shaw G. (1986) *Proc. Natl. Acad. Sci. U.S.A. 83*, 2056−2060.
64. Ohnishi, T. Personnal communication.
65. Williamson, G., and Edmondson, D. (1985) *Biochemistry 24*, 7790−7797.
66. Edmondson, D. E., Ackrell, B. A. C., and Kearney, E. B. (1981) *Arch. Biochem. Biophys. 208*, 69−74.
67. Ohnishi, T., King, T. E., Salerno, J. C., Blum, H., Bowyer, J. R., and Maida, T. (1981) *J. Biol. Chem. 256*, 5577−5582.
68. Beinert, H., Ackrell, B. A. C., Kearney, E. B., and Singer, T. P. (1975) *Eur. J. Biochem. 54*, 185−194.
69. Ackrell, B. A. C., Kearney, E. B., and Edmondson, D. (1975) *J. Biol. Chem. 250*, 7114−7119.
70. Ackrell, B. A. C., Cochran, B., and Cecchini, G. (1989) *Arch. Biochem. Biophys. 268*, 26−34.
71. Tielens, A. G. M. (2000) *Acta Parasitol. 45*, 59−66.

BI010889B